Synthesis of polysulfanilamide by electro polymerization and its corrosion protective properties on 316L stainless steel in 0.2 M HCl

S.A. Habeeb[1] and H.A. Almashhadani[2,3]*

[1]Department of chemistry, College of Education for pure science (Ibn Al-Haitham), University of Baghdad, Baghdad, 10011, Iraq
[2]Dentistry Department, Al-Rasheed University College, Baghdad, 10011, Iraq
[3]College of technical engineering, The Islamic University, Najaf, 54001, Iraq
**E-mail: H_R200690@yahoo.com*

Abstract

The electrochemical polymerization of the monomer sulfanilamide (SAM) in an aqueous solution at room temperature produces polysulfanilamide (PSAM). The Fourier Transform Infrared spectroscopy (FTIR) was used to investigate the properties of the prepared polymer layer that generated on the stainless steel (St.S) surface (working electrode) and Atomic Force Microscope (AFM) was used to characterize the morphology, topology, and detailed surface structure of polymer layer that generated on the surface. The corrosion behavior of uncoated and coated St.S were evaluated by using the electrochemical polarization method in a 0.2 M HCl solution and a temperature range of 293–323 K, the anticorrosion action of the polymer coating on stainless steel was investigated. For the corrosion of St.S, kinetic and thermodynamic activation parameters were estimated. The effect of nanomaterials was investigated by adding them to a monomer solution to improve the anticorrosion performance of polymeric films. Graphene and nano-ZnO were used as nanomaterials in this investigation. The protection efficiency of PSAM increases with the addition of nanomaterials (Graphene and nano zinc oxide) to the monomer solution, particularly graphene, and decreases with increasing temperature (293–323 K). The values of apparent activation energies increase with the addition of different nanomaterials to the coating.

Received: March 9, 2022. Published: April 18, 2022 doi: 10.17675/2305-6894-2022-11-2-11

Keywords: *corrosion, electro polymerization, stainless steel, coating, sulfanilamide nanomaterial.*

1. Introduction

The use of conductive polymers to protect alloys has piqued the interest of several researchers in recent years, who have investigated the protective influence of various chemically or electrochemically synthesized conductive polymers on metal surfaces [1–7]. Electrochemical polymerization has the advantage of being a one-step method, good adhesion, time-saving, and controllable process compared to chemical polymerization [8]. The electrochemical

polymerization method involves oxidation of the monomer to produce radicals, then those radical cations react with each other, or with another monomer, to produce a radical dimer, which is transferred to a trimer and a longer chain length [9, 10]. The efficiency of these protective coatings, which provide thin, tough, and durable barriers to the metal substrate, depends on many factors, like the suitability of organic materials, the corrosive environment, and deposition techniques [11]. A conductive polymer obtained from electrodeposition was used to prevent stainless steel from corrosion in a corrosive medium by interacting with the steel substrate to form a native layer to inhibit the corrosion process. Adding nanomaterials to conductive polymers is one of the interesting ways to improve the protective coating on metals and alloys against corrosion. These polymers with established nanomaterials often offer enhanced electrical, mechanical, and corrosion-resistant properties [12, 13]. In this study, poly sulfanilamide (PSAM) was prepared by electrochemical polymerization of the monomer (SAM) on a St.S surface. The characterization of the polymer film (PSAM) was identified by using AFM and FTIR techniques. The corrosion behavior of uncoated and coated St.S in acidic solutions at different temperatures was studied by adding a nanomaterial (n-ZnO, Graphene) to improve the coating by polymer against corrosion.

2. Experimental part

2.1. Electrochemical polymerization of the monomer (SAM)

To electropolymerize SAM on the St.S (anodic electrode) surface, a standard (DC) power supply was used, with distilled water and acetone; the electrodes were cleaned and washed. Polymerization solutions are made by dissolving 0.1 g of monomer (SAM) in 100 ml of distilled water and adding 3 drops of H_2SO_4 (95% concentration) as a support electrolyte [14]. At room temperature, the polymeric films were deposited on an anodic surface. A further 0.004 g of graphene was added to the monomer solution after dispersion, as well as 0.04 g of nano-ZnO, to improve the coating film's corrosion resistance.

2.2. Corrosion study

For corrosion study: three-electrodes as cell including (working electrode St.S, coated, or non-coated), reference electrode (SCE) and auxiliary electrode (platinum electrode), Anodic and cathodic polarization for corrosion of St.S were performed under potentiostatic conditions in (0.2 M) HCl for coated and uncoated St.S at temperatures ranging from 293 K to 323 K for coated and uncoated St.S.

2.3. Surface characterizations

The polymeric film (PSAM) produced on St.S. has been characterized using a variety of techniques. The Fourier Transform Infrared spectroscopy (FTIR) was used to obtain structural and chemical information of of SAM and PSAM coatings produced on St.S utilizing a Perkin Elmer 2000 system spectrometer in the range 4000–400 cm^{-1}. The surface

topography of SAM and PSAM coating were measured and analyzed by AFM (model: AA3000 Angstrome advanced Inc. USA).

3. Results and Discussion

3.1. FT-IR analysis

The structure of the polymer (PSAM) is shown in Figure 1(B). It was prepared by the electrochemical polymerization of the monomer (SAM) shown in Figure 1(A) and examined by Fourier Transform Infrared spectroscopy (FTIR). The absorption bands of the monomer (SAM) showed the band of O=S=O appeared at (2669.30, 2636.51) cm^{-1}, the absorption of the $–NH_2$ amine group was represented at 3269.12 cm^{-1} symmetric and asymmetric at 3373.27 cm^{-1}. The peaks at 3066.61 cm^{-1} were attributed to the aromatic C–H. In Figure 1(B), we noticed the disappearance of the $–NH_2$ amine group, which confirms the formation of PSAM. The bands are comparatively broad because the polymer PSAM has a broad chain-end distribution [15–18].

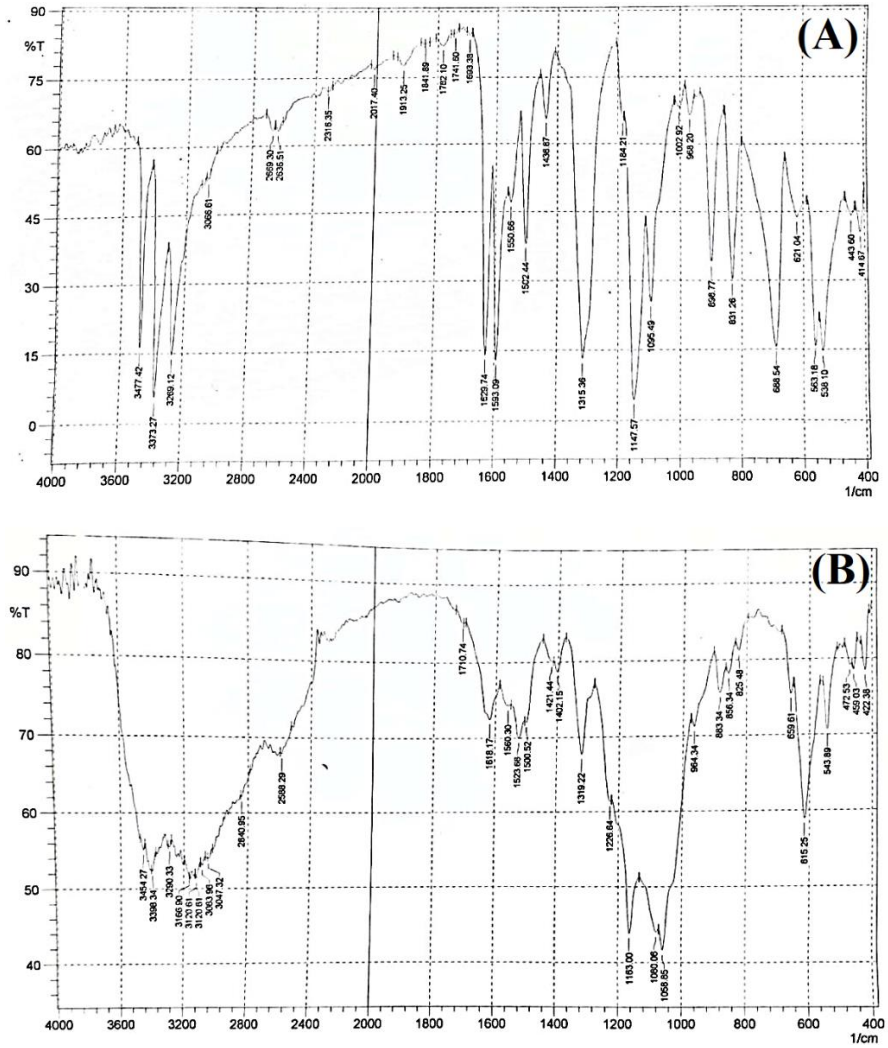

Figure 1. FT-IR for A – the monomer (SAM), B – the polymer (PSAM).

3.2. Atomic force microscope (AFM)

The surface morphology of the St.S coated with PSAM in the absence and presence of nanomaterials (graphene and nano ZnO) was investigated through the AFM technique. The 3D views of the AFM images of all applied coated films (Figure 2) reveal that the topography structure is homogenously covered for all coated films with granular surfaces. The more regular grains may lead to more protective results. In the AFM analysis, The diameter average, roughness average (*Ra*), and Root Mean Square (*RMS*) are the most important parameters used in AFM analysis to characterize surface roughness. Those parameters are represented in Table 1. The results indicate that there is a decrease in the surface roughness of a coated film after the addition of nanomaterials (graphene and nano-ZnO). Were calculated [19, 20].

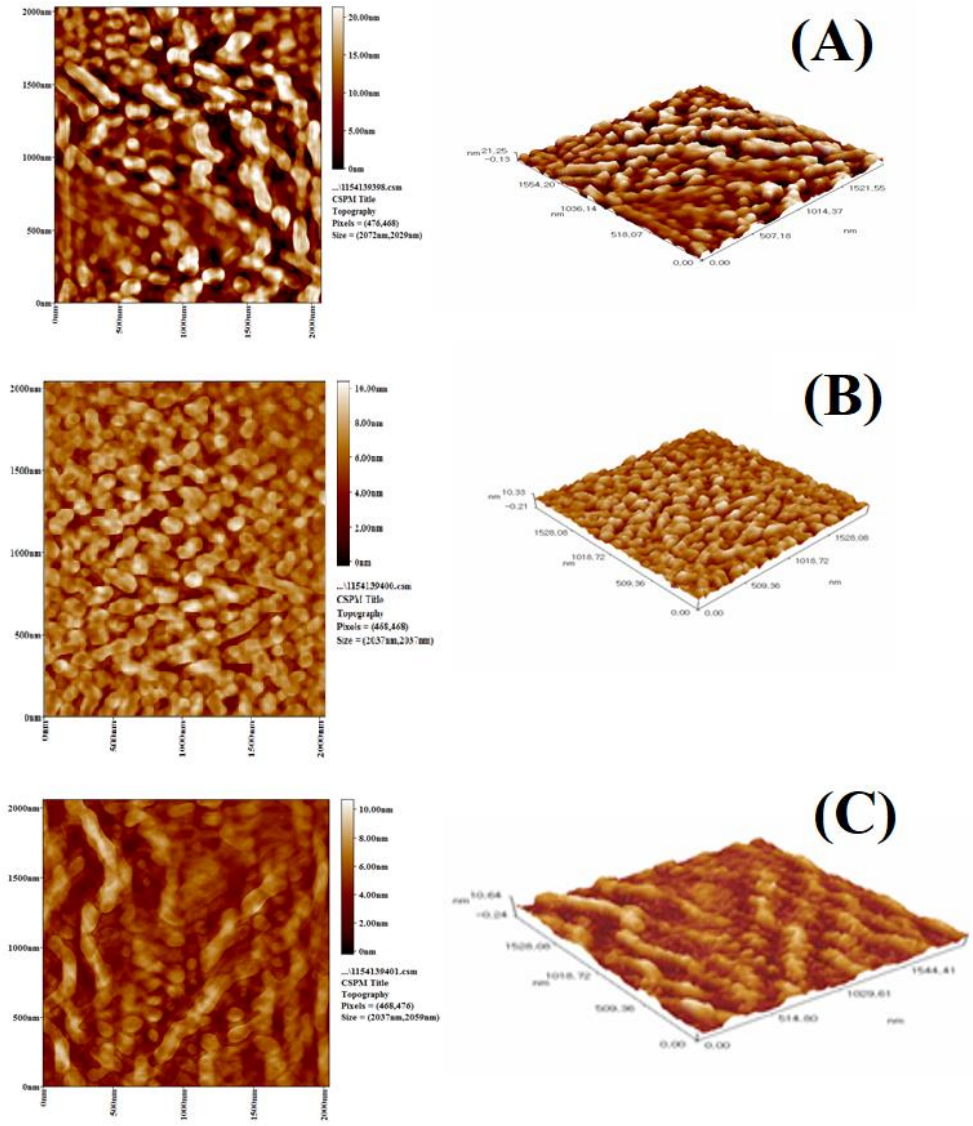

Figure 2. AFM images for (A) stainless steel coated PSAM without Nano material, (B) stainless steel coated PSAM with Graphene, (C) stainless steel coated PSAM with n-ZnO Nano.

Table 1. Average Diameter, Average roughness (*Ra*) and Root Mean Square (*RMS*) values.

Coating	Avg. Diameter	*Ra* (nm)	*RMS* (nm)
PSAM	73.42	4.58	5.46
PSAM&Graphene	89.88	1.11	1.38
PSAM&ZnO	91.96	1.08	1.32

3.3. Corrosion measurements

The influence of polymeric coating films on the anodic and cathodic polarization curves for the corrosion of stainless steel HCl solution was studied at temperatures ranging from 293 K to 323 K. The influence of adding various nanomaterial compounds [grapheme, nano-ZnO] to the monomer solutions on the corrosion of uncoated and coated stainless steel (PSAM) in HCl solution is shown in Figure 3. The corrosion current density (I_{corr}) was determined by extrapolation of anodic and cathodic Tafel plots, and the influence of polymeric coating in the presence and absence of nanomaterials on the corrosion parameter of the stainless steel is shown in Table 2. This parameter includes corrosion current density (I_{corr}), corrosion potential (E_{corr}), anodic Tafel slope (β_a) and cathodic Tafel slope (β_c), weight loss, penetration loss, polarization resistance (R_p), protection efficiency (*PE*%), and porosity (ρ %). The polarization resistance (R_p) can be calculated according to the following equation (1) [21, 22].

$$R_p = \frac{\beta_a \cdot \beta_c}{2.303\left(\beta_a + \beta_c\right)} I_{corr} \tag{1}$$

while the protection efficiency (*PE*%) can be calculated from equation (2) [23],

$$PE\% = \left[1 - \frac{I_{corr}}{I^0_{corr}}\right] \cdot 100 \tag{2}$$

where I^0_{corr} and I_{corr} are the corrosion rates of uncoated and coated stainless steel, respectively.

The porosity of the polymeric films is calculated using the following equation (3) [24].

$$\rho\% = \frac{R_{p,s}}{R_p} \cdot 10^{-\left(\frac{\Delta E_{corr}}{\beta_a}\right)} \tag{3}$$

where $R_{p,s}$ and R_p the represent polarization resistance for uncoated St.S and coated St.S, respectively, E_{corr} is the difference in potential between them.

It is clear from the result data in Table 2 that the E_{corr} of coated St.S by PSAM was shifted to more positive values, and the corrosion current density increased with increasing the temperature, but it decreased after adding nanomaterials to the monomer solution, which led to an increase in the protection effect for St.S corrosion. After the (PSAM) film was

crafted with nanomaterial coated on the St.S, the E_{corr} shifted to the noble direction, the R_p values increased, and the (ρ%) values of the polymeric film decreased. This is because the incorporation of nanomaterial into polymer coatings can greatly improve the barrier impact by decreasing the porosity and zigzagging the diffusion pathway for corrosive ions [25, 26], The lower the value of porosity, the higher the value of polarization resistance.

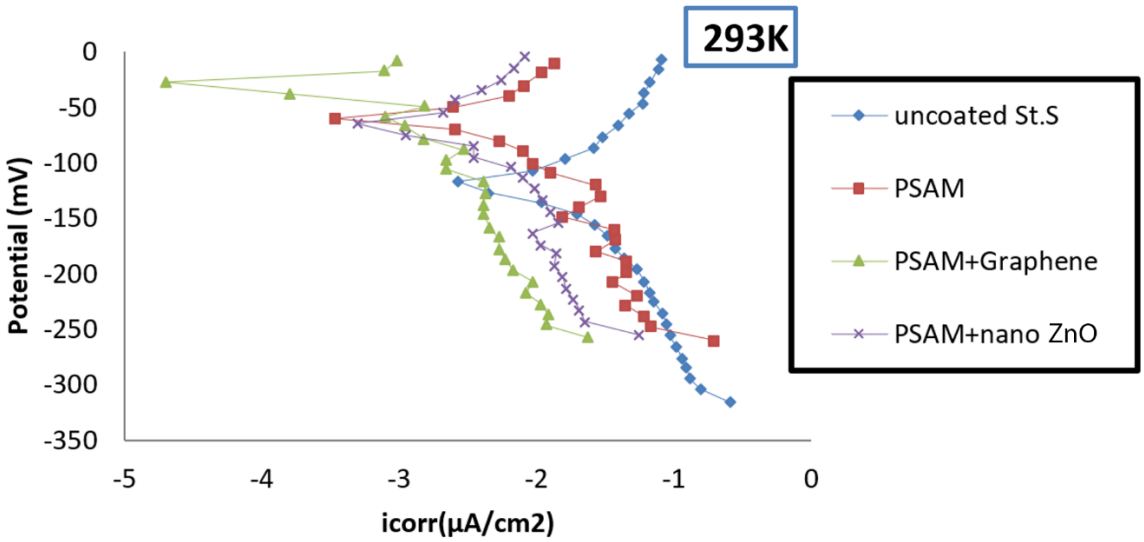

Figure 3. Tafel plot for the corrosion of uncoated stainless steel & coated St.S with PSAM in 0.2 M HCl solution at 293 K.

Table 2. St.S Corrosion parameters in 0.2 M HCl with and without coating at different temperature.

Coating	*T*/K	$-E_{corr}$ mV	I_{corr} µA/cm²	$-\beta_c$ mV/Dec	β_a mV/Dec	*PE*%	*WL* g/m²·d	*PL* mm/y	R_p Ω·cm²	ρ%
Uncoated St.S	293	116.7	18.42	188.7	159.8	–	1.48	0.20	2039.681	
	303	126.0	21.37	199.1	185.8	–	1.72	0.23	1952.858	
	313	206.6	24.35	207.7	220.5	–	1.96	0.27	1906.821	
	323	271.8	25.89	171.6	258.5	–	2.08	0.28	1729.746	
Coated St.S with PSAM	293	59.2	3.89	91.6	91.4	78.88	0.313	0.0423	5106.779	27.87
	303	80.4	5.31	79.7	88.7	75.15	0.427	0.0577	3432.823	
	313	99.2	8.41	77.9	105.6	65.46	0.677	0.0915	2314.597	
	323	129.1	11.01	96.6	117.5	57.47	0.886	0.120	2090.822	
Coated St.S with PSAM modified with Graphene	293	20.0	0.913	194.6	164.0	95.04	0.074	0.0099	42326.43	2.631
	303	94.0	0.947	182.9	181.6	95.57	0.076	0.0103	41781.89	
	313	100.1	1.48	174.0	166.3	93.92	0.119	0.0161	24947.32	
	323	117.5	2.26	184.9	189.5	91.27	0.182	0.0246	17980.75	

Coating	*T*/K	$-E_{corr}$ mV	I_{corr} μA/cm²	$-\beta_c$ mV/Dec	β_a mV/Dec	*PE*%	*WL* g/m²·d	*PL* mm/y	R_p Ω·cm²	ρ%
Coated St.S with PSAM modified with nano-ZnO	293	64.3	1.81	83.2	94	90.17	0.146	0.0197	10588.02	13.88
	303	64.8	2.36	98.2	95.7	88.96	0.190	0.0257	8917.429	
	313	62.1	3.54	115.8	125.3	85.46	0.285	0.0385	7381.85	
	323	65.9	5.65	184.1	160.5	78.18	0.455	0.0615	6589.784	

3.4. Kinetic and thermodynamic of activation parameters

The influence of temperature on the corrosion rate of St.S in the presence and absence of different coatings by PSAM at temperatures ranging from 293–323 K was studied. The Arrhenius equation (4, 5) was used to calculate the apparent activation energies as shown in Figure 4 [27].

$$C.R = \left[A \exp\left(\frac{-E_a}{RT} \right) \right] \cdot 100 \tag{4}$$

$$\log C.R = \log A - \frac{-E_a}{2.303RT} \tag{5}$$

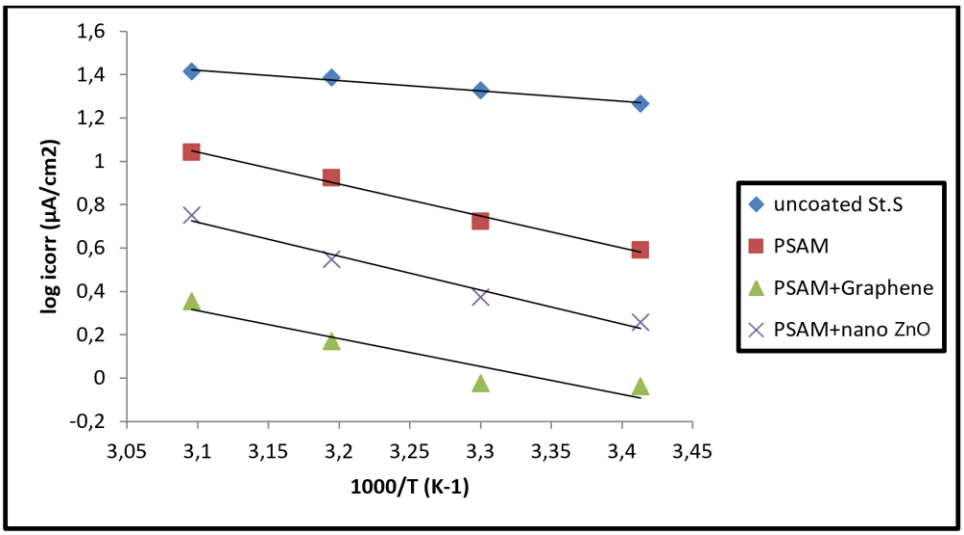

Figure 4. Plot of log i_{corr} *vs.* 1/*T* for uncoated & coated St.S with PSAM in the presence and the existence 0f the nano-materials in 0.2 M HCl.

The values of the entropy of activation (ΔS^*) and the enthalpy of activation (ΔH^*) for the corrosion of uncoated and coated St.S were estimated from (Figure 5) from the transition state equation (6, 7).

$$C.R = \frac{RT}{Nh}\exp\left(\frac{\Delta S^*}{R}\right)\exp\left(\frac{-\Delta H^*}{RT}\right) \quad (6)$$

$$\left(\log\frac{C.R}{T}\right) = \log\frac{R}{Nh} + \frac{\Delta S^*}{2.303R} - \frac{\Delta H^*}{2.303RT} \quad (7)$$

while the values of the activation free energy ΔG^* were calculated by using Gibbs equation (8) [28].

$$\Delta G^* = \Delta H^* - T\Delta S^* \quad (8)$$

where $C.R$ is the corrosion rate, A the pre-exponential factor, E_a the apparent activation energy, T the absolute temperature, R the gas constant (8.314 J·mol^{-1}·K^{-1}), h Plank's constant (6.626176·10^{-34} JS), N is Avogadro's number (6.022·10^{23} mol^{-1}), ΔS^* the entropy of activation, ΔH^* the enthalpy of activation, and ΔG^* the Gibbs free energy.

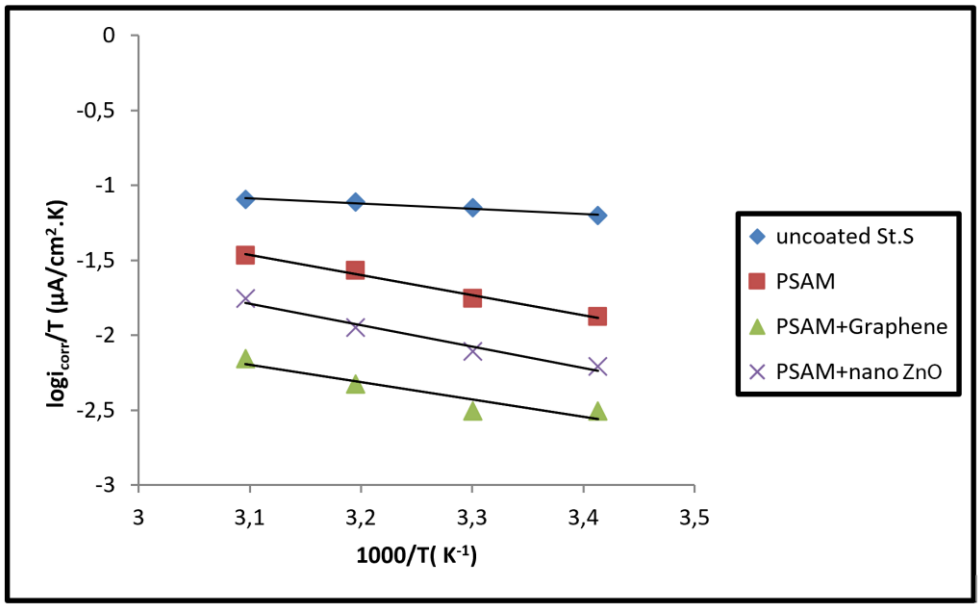

Figure 5. Plot of logi_{corr}/T versus 1/T for uncoated and coated St.S with PSAM in the presence and absence of nanomaterials in 0.2 M HCl.

The results in Table 3 show that the thermodynamic activation functions (ΔH and E_a) for coated St.S had higher values than uncoated St.S, indicating a higher energy barrier. For both uncoated and coated St.S, the activation entropy (ΔS^*) is negative. That means, the activated complex in the determining steps represents the association instead of the dissociation step, which refers to decreases in disorder and goes from the reactant to the activated complex [29]. The values of (ΔG^*) in Table 3 show positive values and show small changes with the increase in the temperature, which indicates the fact that the activated complex is unstable and the likelihood of formation decreases with the increase in the temperature. Furthermore, the (ΔG^*) values for coated St.S show that the activated complex becomes less stable than uncoated St.S.

Table 3. Transition state thermodynamic parameter at different temperatures for the corrosion of uncoated and coated St.S with PSAM film in absence and presence nanomaterials in 0.2 M HCl solution.

Coating	R^2	E_a kJ·mol^{-1}	A/Molecule cm^{-2}·s^{-1}	R^2	ΔH^* kJ·K^{-1}·mol^{-1}	$-\Delta S^*$ J·K^{-1}·mol^{-1}	ΔG^* kJ·K^{-1}·mol^{-1}
Uncoated St.S	0.9789	9.103	$4.721 \cdot 10^{26}$	0.958	6.546	198.112	64.593
							66.574
							68.555
							70.536
Coated St.S with PSAM	0.991	28.183	$2.429 \cdot 10^{29}$	0.9891	25.627	146.653	68.596
							70.063
							71.529
							72.996
Coated St.S with PSAM+ Graphene	0.8992	24.698	$1.226 \cdot 10^{28}$	0.8785	22.141	171.030	72.253
							73.963
							75.673
							77.384
Coated St.S with PSAM+ nano ZnO	0.9782	29.942	$2.221 \cdot 10^{29}$	0.9744	27.386	146.937	70.439
							71.908
							73.377
							74.847

Conclusion

The PSAM synthesis by electro polymerization of SAM on St.S was acted as a good anti-corrosion coating in HCl solution. The protection efficiency of polymer PSAM increases with the addition of nanomaterials to the monomer solution, particularly graphene, and decreases with increasing temperature 293–323 K. The values of apparent activation energies increase with the addition of different nanomaterials to the coating, which indicates an increase in the energy barrier of the corrosion reaction, the positive sign of the activation enthalpies (ΔH^*) for uncoated and coated St.S indicates the endothermic nature of the transition state reaction of St.S. The values of ΔS^* for the uncoated and coated St.S are negative. This means that the activation complex in the rate-determining step represents association rather than dissociation, indicating that a decrease in disordering takes place from the reactant to the activated complex. The positive values of ΔG^* were recorded, listed in Table 3 showing that there was a slight change as the temperature was increased and indicating the non-spontaneous nature of the transition state for uncoated and coated St.S.

The AFM analysis for PSAM with and without nanomaterial (graphene, ZnO) shows the grain size for the polymer decreased after modification with nanomaterial.

References

1. H.A. Al-Mashhadani and K.A. Saleh, Electro-polymerization of poly Eugenol on Ti and Ti alloy dental implant treatment by micro arc oxidation using as Anti-corrosion and Anti-microbial, *Res. J. Pharm. Technol*., 2020, **13**, no. 10, 4687–4696. doi: 10.5958/0974-360X.2020.00825.2
2. M.M. Kadhim, H.A. Al-Mashhadani, R.D. Hashim, A.A. Khadom, K.A. Salih and A.W. Salman, Effect of Sr/Mg co-substitution on corrosion resistance properties of hydroxyapatite coated on Ti–6Al–4V dental alloys, *J. Phys. Chem. Solids*, 2022, **161**, 110450. doi: 10.1016/j.jpcs.2021.110450
3. H.A. AlMashhadani, Synthesis of a CoO-ZnO nanocomposite and its study as a corrosion protection coating for stainless steel in saline solution, *Int. J. Corros. Scale Inhib*., 2021, **10**, no. 3, 1294–1306. doi: 10.17675/2305-6894-2021-10-3-26
4. Y. Situ, W. Ji, C. Liu, J. Xu and H. Huang, Synergistic effect of homogeneously dispersed PANI-TiN nanocomposites towards long-term anticorrosive performance of epoxy coatings, *Prog. Org. Coat*., 2019, **130**, 158–167. doi: 10.1016/J.PORGCOAT.2019.01.034
5. X. Yin, P. Mu, Q. Wang and J. Li, Superhydrophobic ZIF-8-based dual-layer coating for enhanced corrosion protection of Mg alloy, *ACS Appl. Mater. Interfaces*, 2020, **12**, no. 31, 35453–35463. doi: 10.1021/acsami.0c09497
6. C. Wang, X. Sun, L. Yang, D. Song, Y. Wu, T. Ohsaka, F. Matsumoto and J. Wu, In Situ Ion-Conducting Protective Layer Strategy to Stable Lithium Metal Anode for All-Solid-State Sulfide-Based Lithium Metal Batteries, *Adv. Mater. Interfaces*, 2021, **8**, no. 1, 2001698. doi: 10.1002/admi.202001698
7. A. Adhikari, S. De, D. Rana, J. Nath, D. Ghosh, K. Dutta, S. Chakraborty, S. Chattopadhyay, M. Chakraborty and D. Chattopadhyay, Selective sensing of dopamine by sodium cholate tailored polypyrrole-silver nanocomposite, *Synth. Met*., 2020, **260**, 116296. doi: 10.1016/j.synthmet.2020.116296
8. M. Ates, A review on conducting polymer coatings for corrosion protection, *J. Adhes. Sci. Technol*., 2016, **30**, no. 14, 1510–1536. doi: 10.1080/01694243.2016.1150662
9. N.K. Guimard, N. Gomez and C.E. Schmidt, Conducting polymers in biomedical engineering, *Prog. Polym. Sci*., 2007, **32**, no. 8–9, 876–921. doi: 10.1016/j.progpolymsci.2007.05.012
10. J. Li, Y. He, Y. Sun, X. Zhang, W. Shi and D. Ge, Synthesis of polypyrrole/V_2O_5 composite film on the surface of magnesium using a mild vapor phase polymerization (VPP) method for corrosion resistance, *Coatings*, 2020, **10**, no. 4, 402. doi: 10.3390/coatings10040402

11. J.M. Pringle, O. Ngamna, J. Chen, G.G. Wallace, M. Forsyth and D.R. MacFarlane, Conducting polymer nanoparticles synthesized in an ionic liquid by chemical polymerization, *Synth. Met*., 2006, **156**, no. 14–15, 979–983. doi: 10.1016/j.synthmet.2006.06.009
12. R. Gangopadhyay and A. De, Conducting polymer nanocomposites: a brief overview, *Chem. Mater*., 2000, **12**, no. 3, 608–622. doi: 10.1021/cm990537f
13. H.A. AlMashhadani and K.A. Saleh, Corrosion protection of pure titanium implant in artificial saliva by electro-polymerization of poly eugenol, *Egypt. J. Chem*., 2020, **63**, no. 8, 2803–2811. doi: 10.21608/EJCHEM.2019.13617.1842
14. W.S. Hummers and R.E. Offeman, Preparation of graphitic oxide, *J. Am. Chem. Soc*., 1958, **80**, no. 6, 1339. doi: 10.1021/ja01539a017
15. N. Koj, *Infrared abstraction spectroscopy*, Nankodo Company Limited, Tokyo, 1962.
16. F.I. Aljabari and Y.K. Al-Bayati, Estimation of Trimethoprim by using a New Selective Electrodes dependent on Molecularly Imprinted Polymer, *Egypt. J. Chem*., 2021, **64**, no. 10, 6089–6096. doi: 10.21608/EJCHEM.2021.72564.3617
17. R.M. Silverstein and G.C. Bassler, Spectrometric identification of organic compounds, *J. Chem. Educ*., 1962, **39**, no. 11, 546. doi: 10.1021/ed039p546
18. H.A. AlMashhadani and K.A. saleh, Electrochemical Deposition of Hydroxyapatite Co-Substituted By Sr/Mg Coating on Ti-6Al-4V ELI Dental Alloy Post-MAO as Anti-Corrosion, *Iraqi J. Sci*., 2020, **61**, no. 11, 2751–2761. doi: 10.24996/ijs.2020.61.11.1
19. H.A. Almashhadani, M.K. Alshujery, M. Khalil, M.M. Kadhem and A.A. Khadom, Corrosion inhibition behavior of expired diclofenac Sodium drug for Al 6061 alloy in aqueous media: Electrochemical, morphological, and theoretical investigations, *J. Mol. Liq*., 2021, **343**, 117656. doi: 10.1016/j.molliq.2021.117656
20. P. Karthikeyan, M. Malathy and R. Rajavel, Poly(ophenylenediaminecoaniline)/ZnO coated on passivated low nickel stainless steel, *J. Sci.: Adv. Mater. Devices*, 2017, **2**, no. 1, 86–92. doi: 10.1016/j.jsamd.2016.11.003
21. H. Almashhdani and K. Alsaadie, Corrosion Protection of Carbon Steel in seawater by alumina nanoparticles with poly (acrylic acid) as charging agent, *Moroccan J. Chem*., 2018, **6**, no. 3, 455-465. doi: 10.48317/IMIST.PRSM/morjchem-v6i3.6214
22. E. Bardal, *Corrosion and protection*, London, 2004.
23. M.A. Aal, S. Radwan and A. El-Saied, Phenothiazines as corrosion inhibitors for zinc in NH_4Cl solution, *Br. Corros. J*., 1983, **18**, no. 2, 102–106.
24. O. Girčienė, R. Ramanauskas, L. Gudavičiūtė and A. Martušienė, The effect of phosphate coatings on carbon steel protection from corrosion in a chloride-contaminated alkaline solution, *Chemija*, 2013, **24**, no. 4, 251–259.
25. A. Nazari, A. Pruna, C. Goran-Granqvist, F. Pacheco-Torgal and S. Amirkhanian, Contributor contact details, *Nanotechnol. Eco-Effic. Constr. (2nd Ed.)*, 2019. doi: 10.1016/B978-0-85709-544-2.50019-1
26. F.F. Fang, H.J. Choi and J. Joo, Conducting polymer/clay nanocomposites and their applications, J. Nanosci. Nanotechnol., 2008, **8**, no. 4, 1559–1581.

27. S. Umoren, I. Obot, E. Ebenso and N. Obi-Egbedi, The Inhibition of aluminium corrosion in hydrochloric acid solution by exudate gum from *Raphia hookeri*, *Desalination*, **2009**, 247, no. 1–3, 561–572. doi: 10.1016/j.desal.2008.09.005
28. M.G. Fontana and N.D. Greene, *Corrosion Engineering*, 1967. doi: 10.1016/C2012-0-03070-0
29. G. Avci, Corrosion inhibition of indole-3-acetic acid on mild steel in 0.5M HCl, *Colloids Surf., A*, 2008, **317**, no. 1–3, 730–736. doi: 10.1016/j.colsurfa.2007.12.009

♦ ♦ ♦